Applied Physics Letters

Measurement of electrical contact resistance at nanoscale gold-graphite interfaces

Cite as: Appl. Phys. Lett. **115**, 091602 (2019); https://doi.org/10.1063/1.5109880
Submitted: 13 May 2019 . Accepted: 10 August 2019 . Published Online: 26 August 2019

Mohammad R. Vaziriserehk, Saima A. Sumaiya, Ashlie Martini, and Mehmet Z. Baykara

Applied Physics Letters ARTICLE scitation.org/journal/apl

Measurement of electrical contact resistance at nanoscale gold-graphite interfaces

Cite as: Appl. Phys. Lett. **115**, 091602 (2019); doi: 10.1063/1.5109880
Submitted: 13 May 2019 · Accepted: 10 August 2019 ·
Published Online: 26 August 2019

Mohammad R. Vazirisereshk,[a] Saima A. Sumaiya,[a] Ashlie Martini,[b] and Mehmet Z. Baykara[b]

AFFILIATIONS

Department of Mechanical Engineering, University of California Merced, Merced, California 95343, USA

[a]**Contributions:** M. R. Vazirisereshk and S. A. Sumaiya contributed equally to this work.
[b]**Authors to whom correspondence should be addressed:** amartini@ucmerced.edu and mehmet.baykara@ucmerced.edu

ABSTRACT

An approach to measuring electrical contact resistance as a direct function of the true contact size at the nanoscale is presented. The approach involves conductive atomic force microscopy (C-AFM) measurements performed on a sample system comprising atomically flat interfaces (up to several hundreds of nanometers in lateral size) formed between gold islands and a highly oriented pyrolytic graphite (HOPG) substrate. The method overcomes issues associated with traditional C-AFM such that conduction can be correlated with a measurable true, conductive contact area. Proof-of-principle experiments performed on gold islands of varying size point toward an increasing contribution of the island-HOPG junction to the measured total resistance with decreasing island size. Atomistic simulations complement and elucidate experimental results, revealing the maximum island size below which the electrical contact resistance at the island-HOPG junction can be feasibly extracted from the measured total resistance.

Electrical contact resistance (ECR) plays an important role in the function and performance of electromechanical components used in many applications, including switches/relays and connectors. Performance criteria significantly affected by ECR in such devices include insertion loss, Joule heating, and lifetime. Beyond its relevance on conventional engineering length scales, ECR is critical for the development of electromechanical components at the micrometer scale due to the significant effect of surfaces at such small length scales. Therefore, ECR is of concern for current and emerging microscale electromechanical components, e.g., microswitches being developed for applications ranging from radar technologies to wireless communications.[1,2] Such microscale electromechanical devices conduct electricity through much smaller scale contact patches, due to the rough, multiasperity character of the involved surfaces.[1,3,4] In fact, numerical and analytical studies of contacts formed at individual asperities in microswitches with gold contacts revealed that the typical true contact size ranges from a few nanometers to hundreds of nanometers, depending on the contact forces involved.[5] Consequently, measuring ECR accurately at these length scales is important for emerging microelectromechanical applications.

For fundamental studies of ECR at submicrometer length scales, researchers typically use conductive atomic force microscopy (C-AFM), where a conductive AFM tip is used to scan a surface in contact mode (where repulsive interaction forces are typically kept constant at the level of a few nanoNewton via feedback loops), under the application of a bias voltage (V) between the AFM tip and the sample.[6] During scanning, two complementary data maps are obtained: a topography map which provides nanometer scale information about the structure of the surface and a current (I) map, where the amount of current flowing between the tip and the sample is measured as a function of position on the sample surface. Using such information, the electrical conductance/resistance of the surface can be characterized with nanometer scale spatial resolution. Moreover, the tip can be fixed at a given position on the sample surface and the bias voltage varied such that the current is recorded as a function of bias voltage in the form of I-V curves, which provides further information about the electrical properties of the sample.[7]

The method of C-AFM described above has been used to study the electrical properties of many different materials over the past couple of decades.[8] However, despite the relatively wide-spread use of the method, there are significant drawbacks associated with traditional C-AFM. First, wear of the tip apex during extended periods of scanning, especially when trying to achieve large contact sizes by applying large normal loads, can cause measured resistance values to change over time.[9] Second,

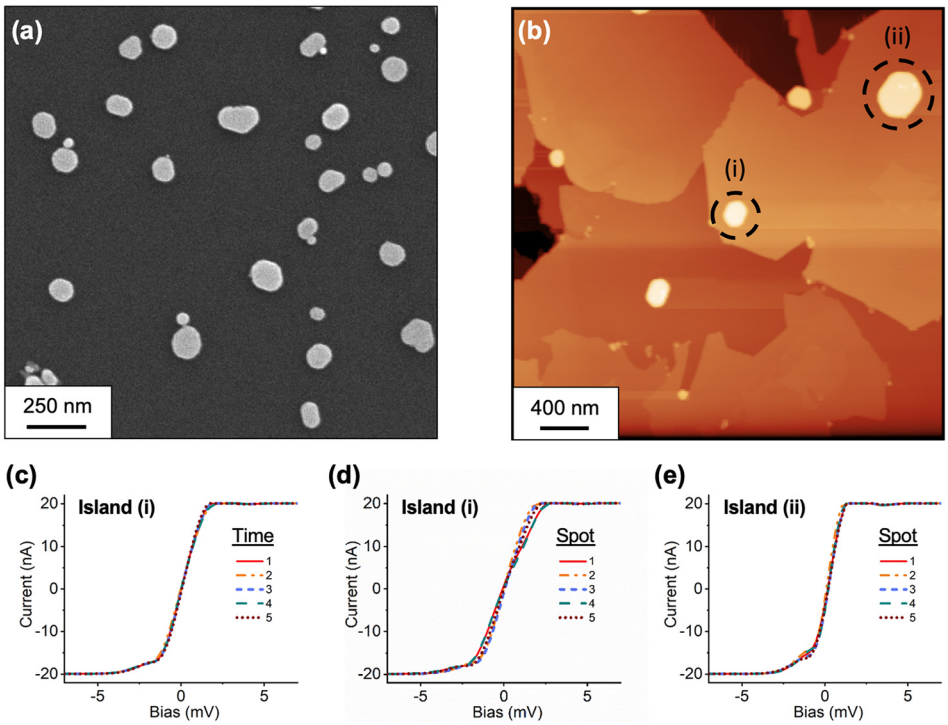

FIG. 1. (a) A representative SEM image of the sample system consisting of gold islands on HOPG. (b) AFM image of several gold islands on HOPG. Two gold islands (of size 34 800 nm^2 and 111 900 nm^2) on which *I-V* measurements are performed are highlighted with dashed circles and indicated as (i) and (ii), respectively. (c) Five *I-V* curves obtained on an individual spot on island (i) in (b) over a duration of 2 min., demonstrating high reproducibility. Note that the current saturates at 20.0 nA, which is the limit of our measurement setup. (d) Five *I-V* curves obtained on five different spots on island (i) in (b), demonstrating noticeable variability. (e) Five *I-V* curves obtained on five different spots on island (ii) in (b), demonstrating less variability than those obtained on island (i). Please note the larger slope of the *I-V* curves on island (ii) when compared with island (i), indicative of a smaller resistance to electron flow, in accordance with the larger size of the island.

potential oxidation and/or contamination of the tip and the sample during the experiments can lead to lower-than-expected current flow across the interface.[10–12] Third, nanoscale roughness of the tip and/or sample results in "true" conductive contact areas that are much smaller than the "apparent" size of the contact. Finally, lack of information about the geometry of the contact established between the AFM tip and the substrate requires that the contact size be approximated using continuum-based contact mechanics models which may break down at the nanoscale.[7,13,14] All of these hinder the ability to correlate conduction and resistance measured using traditional C-AFM directly to the contact size, which in turn limits the formation of a complete understanding of trends observed in such measurements.

To partially address the issues above, recent studies employed C-AFM on a sample system with microfabricated Pd/Au disks of 100–500 nm radius on a highly oriented pyrolytic graphite (HOPG) substrate.[15–17] During the experiments, the metal-coated tip of the AFM cantilever was "welded" onto a particular metal contact and *I-V* curves were measured to characterize electrical resistance. This approach was used to show that conduction in this size regime is compatible with a diffusive transport model where resistance is inversely proportional to the contact radius.[15] While such an approach is advantageous as the size of the contact can be directly measured via AFM, the roughness as well as the degree of molecular cleanliness at the interface between the Pd/Au disks and the HOPG remains uncharacterized, which prevents unambiguous correlations to be made between the measured resistances and true conductive contact areas. Perhaps more importantly, the experiments were limited to one measurement per island since the tip was welded to the disk prior to testing, preventing measurements to be made on contacts of different sizes with the same probe.

Here, we introduce a C-AFM method that leverages the concept of measuring conductance at nanoscale contacts, where the true contact size is known and multiple measurements of conductance at different contacts can be performed with the same probe. Specifically, the contact of interest is formed by nanoscale gold islands of varying size on HOPG. As the interface that is formed between the gold islands and HOPG has been shown to be atomically flat and molecularly clean following a specific method of preparation,[18] these junctions represent an ideal scenario where ECR can be fundamentally studied, without ambiguities associated with contact geometry and cleanliness encountered in conventional C-AFM experiments. Proof-of-principle experiments introduced here are complemented by molecular dynamics (MD) simulations that enable explicit control of the island and tip size as well as approximation of electrical current. Importantly, the simulations provide guidance for the tip and island sizes needed to effectively implement this method for studies of ECR at nanoscale contacts.

The sample system utilized during the measurements was prepared via a two-step process. First, ZYB-quality HOPG samples (Ted Pella) were cleaved in air and rapidly introduced into the vacuum chamber of a thermal evaporator (Denton Vacuum), where they were covered with a thin layer of 99.999% purity gold for a total deposition amount of 1 Å. The gold-covered HOPG samples were then annealed in a benchtop furnace at a temperature of 650 °C for 120 min. The resulting sample system consisted of individual, crystalline gold islands of varying lateral (up to ~400 nm) and vertical (up to ~90 nm) size on the HOPG substrate [Fig. 1(a)]. The wide variation in the lateral size of the gold islands, which are known to exhibit atomically flat and molecularly clean interfaces with the HOPG substrate,[18] is particularly advantageous for the experiments proposed here, as it allows ECR to

be studied directly as a function of true contact size, overcoming a major limitation of conventional C-AFM experiments.

Once sample preparation and characterization via scanning electron microscopy (SEM) were complete, the sample was imaged via dynamic (i.e., tapping-mode) AFM (Asylum Research, Cypher VRS) to locate individual gold islands of interest for *I-V* spectroscopy [see, e.g., the two islands of different size on the same HOPG terrace highlighted in Fig. 1(b)]. In addition to the fact that AFM imaging allows a precise determination of the area of contact formed between individual gold islands and the HOPG substrate, it can also be employed to determine the island height and to evaluate topographical roughness on the top surface of gold islands (which was measured to be 3.0 ± 1.3 Å (mean ± s.d.) for our sample system), the potential factor that could cause variations in *I-V* curves obtained on different spots on a given gold island. Following AFM imaging, the Ti/Ir-coated conductive cantilever (Asylum Research, ASYELEC.01-R2, tip radius of ∼25 nm as confirmed by SEM imaging) was brought into contact with the surface of individual gold islands at desired locations. *I-V* spectroscopy (whereby the bias voltage was applied to the conductive cantilever) was then performed to assess the electrical conductance across the multijunction contact formed by the tip apex, the gold island, and the HOPG substrate (which is electrically connected to the AFM sample plate via silver paint). The majority of measured *I-V* curves were of Ohmic character around zero bias, with a mostly linear dependence of current on bias voltage. It should be mentioned here that such Ohmic measurements of current as a function of bias voltage were not obtained with all conductive AFM tips, and "blocking" behavior (that involves essentially no current flow up to several volts of bias voltage) was also occasionally observed.[10] For tips that exhibited Ohmic behavior, the total resistance (R_{Total}) was determined by linear fits to the data around zero bias.

As proof-of-principle experiments, multiple *I-V* curves were collected on individual spots on gold islands of varying size, in a bias voltage range of −7.0 mV to +7.0 mV and a small applied normal load of 0.5 nN (it should be noted that for this particular tip, adhesion on the gold islands was on the order of 10.0 nN). Figure 1(c) shows five *I-V* curves recorded consecutively (over a total span of ∼2 min) on an individual spot on island (i) identified in Fig. 1(b) which has an area of 34 800 nm^2, demonstrating high reproducibility. The variability of measurements taken at different spots on a given island was also tested. Figure 1(d) presents representative *I-V* curves collected on five different spots separated by a few tens of nanometers on island (i) that demonstrate noticeable variation, such that R_{Total} (as deduced from a total of 28 curves collected on five different spots) for this particular island was determined to be 93.8 ± 19.2 kΩ. Moreover, Fig. 1(e) shows five *I-V* curves collected on five different spots (again separated by a few tens of nanometer) on another gold island (which is designated as island (ii) in Fig. 1(b) and has an area of 111 900 nm^2), on the same terrace as island (i). R_{Total} for island (ii), as deduced from a total of 28 curves collected on five different spots, was measured as 40.2 ± 1.2 kΩ. As expected, a smaller total resistance was measured on the larger island because of the lower resistance at the island-HOPG junction.

The resistance measurements described above were repeated with two additional pairs of islands with significantly different size, with each pair located on the same HOPG terrace. All measurements were performed with the same tip and at an applied normal load of 0.5 nN, and repeat measurements performed on the first island after the collection of *I-V* curves on both islands were utilized to rule out the potential occurrence of tip changes during the experiments. The results of each set of experiments, summarized in Table I, consistently demonstrated a larger R_{Total} for smaller islands. Note that, while the results for two islands in a given data set can be compared, resistances cannot be compared across the data sets because the islands are on different terraces and HOPG terraces have been reported to exhibit significant differences in resistance.[19]

Interestingly, the larger islands in the three data sets in Table I all exhibited very similar R_{Total} values (40.2 ± 1.2 kΩ, 43.3 ± 5.1 kΩ, and 40.1 ± 1.1 kΩ), despite significant differences in the contact size (111 900 nm^2, 130 900 nm^2, and 61 900 nm^2, respectively). On the other hand, mean R_{Total} values measured on the smaller islands were appreciably different from each other (93.8 ± 19.2 kΩ, 73.4 ± 16.9 kΩ, and 56.1 ± 9.7 kΩ). Also, a particularly interesting observation here was that the standard deviation of R_{Total} on smaller islands was significantly higher than that on larger islands. A potential explanation could involve the superlubric nature of the contact between the gold islands and the HOPG substrate and the associated miniscule barriers to motion experienced by small islands,[18] supported by the observation that the smaller islands tended to move laterally on the HOPG substrate during the collection of *I-V* curves.

To provide explanations for the findings described above, MD simulations were designed to mimic the C-AFM experiments as shown in Fig. 2. The model consisted of a diamond-like carbon (DLC) tip apex in contact with gold islands on an HOPG substrate [Fig. 2(a)]. Three different tips with radii of 3.6, 4.1, and 5.0 nm were brought in contact with gold islands of varying contact areas ranging from 50 to almost 2400 nm^2. The HOPG substrate consisted of two graphene layers having lateral dimensions of 10 × 10, 25 × 20, or 48 × 40 nm^2, depending on the size of the island (lateral size of the HOPG substrate did not affect results). The bottommost graphene layer was fixed and the topmost part of the tip was treated as a rigid body. A normal load of 1.25 nN was applied to the tip. The simulations were performed in the canonical ensemble with the LAMMPS code.[20] The atomic configurations were visualized using OVITO.[21] The Embedded-Atom Method (EAM)[22] was used to model Au-Au interactions and the Adaptive Intermolecular Reactive Empirical Bond Order (AIREBO)[23] potential was used for C-C interactions. The interactions between materials were modeled using the Morse potential for Au-C

TABLE I. Total resistance measured on pairs of gold islands via C-AFM, arranged in three data sets acquired on different days. The island-HOPG resistance for small islands is also reported. Contact radii have been calculated by approximating the island-HOPG contact geometry as circular. For each island, mean and standard deviation values for resistance are deduced from multiple (>10) *I-V* curves recorded on multiple (>2) spots.

Data set	Island size (nm^2)	Island radius (nm)	Total resistance (kΩ)	Island-HOPG resistance (kΩ)
I	111 900	189	40.2 ± 1.2	
	34 800	105	93.8 ± 19.2	53.6 ± 19.2
II	130 900	204	43.3 ± 5.1	
	16 500	72	73.4 ± 16.9	30.1 ± 17.7
III	61 900	140	40.1 ± 1.1	
	23 000	86	56.1 ± 9.7	16.1 ± 10.2

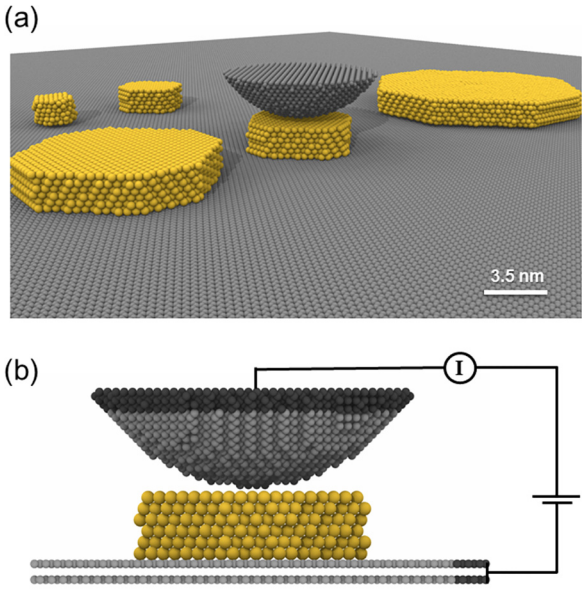

FIG. 2. (a) Perspective view of the MD simulations where a model AFM tip apex comes into contact with gold islands of varying size on a graphite substrate. (b) For each tip-island combination, current between the tip and the edge of the graphite substrate (shown in darker gray) is approximated using the EChemDID method.

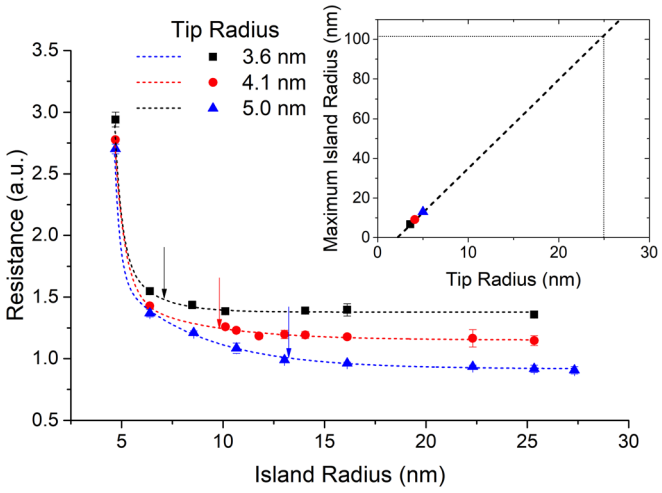

FIG. 3. Total resistance calculated from the simulations as a function of island radius for three different model tips (symbols). The data are fit to an exponential function (dashed lines) to determine the maximum island radius for each tip (arrows), after which the contribution of the island-HOPG resistance to the total resistance becomes negligible (see the text). Inset: Maximum island radius for each model tip (considering island radii where the total resistance is 10% greater than the tip-island resistance) with linear extrapolation to the radius of the tip used in the C-AFM experiments (25 nm).

($D_0 = 0.00832\,eV$, $r_0 = 0.387035$ nm, and $\alpha = 1.25707$).[24] The time step was 1 fs. For each island and tip combination (three tips and twelve islands), equilibration was run until the system reached steady state, defined as the point at which the vertical position of the top rigid part of the tip varied by less than 0.1 Å, which took up to 450 ps. After this point, production simulations were run for another 100 ps, from which atomic configurations were extracted at 0, 25, 50, 75, and 100 ps for use in the current calculations.

For each tip-island combination, the EChemDID[25] method was used to estimate the current between the top of the tip and edge of the graphite, as shown in Fig. 2(b). This method has been successfully used before to study the behavior of nanoswitches[26,27] and C-AFM measurements.[28,29] EChemDID requires the use of a reactive potential, so for the current calculations, the potential for all interatomic interactions was changed to ReaxFF, with parameters for systems containing gold and carbon atoms.[30,31] The atomic configurations taken from the production simulations with the nonreactive potential were used as the starting point for the EChemDID calculations. Note that this approach was used because the large model sizes precluded direct use of ReaxFF for the simulations. For each configuration, EChemDID was run to calculate current and then the average was taken from the five configurations for each tip-island combination. Although EChemDID inherently assumes diffusive transport, this is reasonable for the relatively large island-HOPG contacts modeled here based on an analysis of carrier transport in graphene-metal junctions.[32] Furthermore, any error associated with this assumption for the smaller tip-island contacts is the same for all the models and so will not affect the trends predicted by the simulations.

The results of the total resistance calculated from simulations of three different tips and twelve different islands are shown in Fig. 3. For this model system, if we assume that the resistance within the tip, the island, and the HOPG is small compared to that at the two interfaces, the total resistance is

$$R_{Total} = R_{Tip} + R_{Tip\text{-}Island} + R_{Island} + R_{Island\text{-}HOPG} + R_{HOPG} \approx R_{Tip\text{-}Island} + R_{Island\text{-}HOPG}.$$

Therefore, the resistance observed in Fig. 3 is due to both tip-island and island-HOPG junctions. For large islands, resistance will be dominated by the much smaller tip-island contact, which does not change with the island size, consistent with the near-constant resistance observed for larger islands in Fig. 3. For small islands, the island-HOPG contact contributes appreciably to the total resistance, leading to total resistance values that decrease with increasing island size, again as observed in Fig. 3. For each tip, the resistance-island size data were fit to an exponential function that captured the decrease in resistance with increasing island size for small islands (where both tip-island and island-HOPG resistances contribute) and the constant resistance for large islands (where tip-island contact resistance is dominant). We then identified the island radius corresponding to a total resistance that is 10% greater than the tip-island resistance and assumed this to be the maximum island size for which the total resistance can be differentiated from the tip-island resistance. Using the maximum island size calculated for three model tips, we linearly extrapolated to the tip size range relevant for the experiments, as shown in the inset of Fig. 3. For the 25 nm radius tips employed in C-AFM experiments, this analysis suggested that island radii smaller than 101 nm would be needed to feasibly extract the island-HOPG contact resistance from the measured total resistance. Although the choice of 10% here is arbitrary, other reasonable choices yield similar results, e.g., the maximum island size for the 25 nm tip with a 20% criterion is 75 nm.

The simulation results have significant implications for the C-AFM method reported here: they explain the observation of very similar resistance values for large islands in our experiments, despite significant differences in the size, in contrast to smaller islands where the contribution of the island-HOPG resistance to the total resistance is appreciable. In particular, our experimental results summarized in Table I, when interpreted with the help of MD simulations, point toward a tip-island resistance value on the order of 40 kΩ (as deduced from the measurements on the larger islands in the three data sets, where the contribution of the island-HOPG junction to the measured resistance is negligible). Taking the resistor-in-series model into account, the resistance measured on the big islands can then be subtracted from the resistance measured on smaller islands in each data set, thereby allowing the calculation of the electrical contact resistance at the island-HOPG junction for the smaller islands (see the last column of Table I). Again, these numbers cannot be compared with each other because the islands are on different terraces.[19] Finally, the largest island-HOPG contact radius for which the contribution of the island-HOPG junction to the total resistance can be detected was determined to be 105 nm in our experiments (Table I), reasonably close to the range extrapolated from the MD simulations (75 to 101 nm).

While the results reported above indicate that measurements should be performed on smaller islands to accurately determine ECR at island-HOPG interfaces, an alternative and/or complementary approach could involve the use of tips with large radii, such that the resistance of the tip-island junction is minimized and the relative contribution of the island-HOPG resistance to the total resistance increases. This could, for instance, be achieved by the deliberate blunting of tips prior to the experiments[33,34] or the use of conductive colloidal probes. These avenues will be pursued in future research.

In summary, this study demonstrated an approach to C-AFM aimed at enabling direct correlations between the true contact size and ECR. The approach leveraged the well-defined, atomically flat contact that forms between gold islands and HOPG. Proof-of-principle experiments were supplemented by MD simulations that approximated resistance for model systems in which the exact sizes of both tip-island and island-HOPG contacts were known. The simulations explained the experimental findings that showed a trend of an increasing contribution of the island-HOPG junction to the measured total resistance with decreasing island size. The approach demonstrated here has the potential to contribute to a fundamental understanding of electron conduction mechanisms at small length scales, for instance by enabling an investigation of the transition between the diffusive and ballistic electron transport regimes, with important implications for microscale electromechanical devices.

This work was supported by the Air Force Office of Scientific Research (AFOSR) Award No. FA9550-19-1-0035. The simulations were run using the Extreme Science and Engineering Discovery Environment (XSEDE), which was supported by National Science Foundation (NSF) Grant No. ACI-1548562.

REFERENCES

[1]A. Basu, G. G. Adams, and N. E. McGruer, J. Micromech. Microeng. **26**, 104004 (2016).
[2]F. Giacomzzi and J. Iannacci, in *Handbook of MEMS for Wireless and Mobile Applications*, edited by D. Uttamchandani (Woodhead Publishing, 2013), pp. 225–257.
[3]D. Berman and J. Krim, Prog. Surf. Sci. **88**, 171 (2013).
[4]B. F. Toler, R. A. Coutu, and J. W. McBride, J. Micromech. Microeng. **23**, 103001 (2013).
[5]S. Majumder, N. E. McGruer, G. G. Adams, P. M. Zavracky, R. H. Morrison, and J. Krim, Sens. Actuators, A **93**, 19 (2001).
[6]F. Houzé, R. Meyer, O. Schneegans, and L. Boyer, Appl. Phys. Lett. **69**, 1975 (1996).
[7]V. B. Engelkes, J. M. Beebe, and C. D. Frisbie, J. Phys. Chem. B **109**, 16801–16810 (2005).
[8]A. Avila and B. Bhushan, Crit. Rev. Solid State Mater. Sci. **35**, 38 (2010).
[9]W. Frammelsberger, G. Benstetter, J. Kiely, and R. Stamp, Appl. Surf. Sci. **253**, 3615 (2007).
[10]S. J. O'Shea, R. M. Atta, and M. E. Welland, Rev. Sci. Instrum. **66**, 2508 (1995).
[11]M. A. Lantz, S. J. O'Shea, and M. E. Welland, Rev. Sci. Instrum. **69**, 1757 (1998).
[12]S. B. Vishnubhotla, R. Chen, S. R. Khanal, J. Li, E. A. Stach, A. Martini, and T. D. B. Jacobs, Nanotechnology **30**, 045705 (2019).
[13]T. D. B. Jacobs and A. Martini, Appl. Mech. Rev. **69**, 060802 (2017).
[14]B. Luan and M. O. Robbins, Nature **435**, 929 (2005).
[15]E. Koren, A. W. Knoll, E. Lörtscher, and U. Duerig, Appl. Phys. Lett. **105**, 123112 (2014).
[16]E. Koren, A. W. Knoll, E. Lörtscher, and U. Duerig, Nat. Commun. **5**, 5837 (2014).
[17]E. Koren, I. Leven, E. Lörtscher, A. Knoll, O. Hod, and U. Duerig, Nat. Nanotechnol. **11**, 752 (2016).
[18]E. Cihan, S. İpek, E. Durgun, and M. Z. Baykara, Nat. Commun. **7**, 12055 (2016).
[19]S. Banerjee, M. Sardar, N. Gayathri, A. K. Tyagi, and B. Raj, Phys. Rev. B **72**, 075418 (2005).
[20]S. Plimpton, J. Comput. Phys. **117**, 1 (1995).
[21]S. Alexander, Modell. Simul. Mater. Sci. Eng. **18**, 015012 (2010).
[22]X. W. Zhou, R. A. Johnson, and H. N. G. Wadley, Phys. Rev. B **69**, 144113 (2004).
[23]S. J. Stuart, A. B. Tutein, and J. A. Harrison, J. Chem. Phys. **112**, 6472 (2000).
[24]J. A. de la Rosa-Abad, G. J. Soldano, S. J. Mejía-Rosales, and M. M. Mariscal, RSC Adv. **6**, 77195 (2016).
[25]N. Onofrio and A. Strachan, J. Chem. Phys. **143**, 054109 (2015).
[26]N. Onofrio, D. Guzman, and A. Strachan, Nat. Mater. **14**, 440 (2015).
[27]N. Onofrio, D. Guzman, and A. Strachan, Nanoscale **8**, 14037 (2016).
[28]X. Hu, J. Lee, D. Berman, and A. Martini, Carbon **137**, 118 (2018).
[29]X. Hu and A. Martini, Nanoscale **9**, 16852–16857 (2017).
[30]S. G. Srinivasan, A. C. T. van Duin, and P. Ganesh, J. Phys. Chem. A **119**, 571 (2015).
[31]T. T. Järvi, A. C. T. van Duin, K. Nordlund, and W. A. Goddard, J. Phys. Chem. A **115**, 10315–10322 (2011).
[32]F. Xia, V. Perebeinos, Y. M. Lin, Y. Q. Wu, and P. Avouris, Nat. Nanotechnol. **6**, 179 (2011).
[33]S. B. Vishnubhotla, R. Chen, S. R. Khanal, X. Hu, A. Martini, and T. D. B. Jacobs, Tribol. Lett. **67**, 97 (2019).
[34]B. Gotsmann and M. A. Lantz, Nat. Mater. **12**, 59 (2013).